Supporting Information

Auld et al. 10.1073/pnas.0909141107

SI Text

SI Methods. ***Structure solution and refinement.*** The firefly luciferase protein (Sigma cat. no. L9506) was exchanged to the buffer previously described for crystallization of firefly luciferase (1) (200 mM $(NH_4)_2SO_4$, 1 mM EDTA, 1 mM DTT, 10% glycerol, 25% ethylene glycol, 25 mM Tris pH 7.8) and concentrated to 16.3 mg/mL. Crystallization trials were conducted in Compact Jr. sitting drop vapor diffusion plates (Emerald Biosystems) using 0.5 μL of protein and 0.5 μL of crystallization screen solution equilibrated against 100 μL reservoir solution. Crystals displaying a needle morphology were obtained with 24 h at 4 °C from the Precipitant Synergy screen (Emerald Biosystems) conditions no. 41 (25% PEG 400, 20% PEG 3350, 0.1 M $MgCl_2$, 0.1 M Tris pH 8.5) and no. 45 [30% PEG 1500, 8% (vol/vol) MPD, 0.1 M Tris pH 8.5]. Crystals from Synergy nos. 41 and 45 were soaked for 2 h in fresh drops of crystallization solution containing 5 mM ATP and 5 mM PTC124 to prepare the adduct complex. Luc:Apo and Luc:Apo2 crystals were obtained from Synergy no. 45 and Synergy no. 41, respectively. All samples were frozen in their respective crystallization solutions which also served as a cryoprotectant.

All X-ray diffraction data were collected at the Advanced Photon Source, Industrial Macromolecular Crystallography Association Collaborative Access Team beamline 17BM using an Area Detector Systems Corporation Quantum 210 CCD detector. Data were collected at 100 K using an X-ray wavelength of 1.0000 Å. Data were integrated and scaled using HKL2000 (2). Structural comparison was performed using the least squares fitting procedure in Coot. Cα atoms were used for fitting. Figures were prepared using the Ribbons software package (3).

The unit cell parameters and space group for the luciferase crystals obtained in our laboratory were different from those reported for the two known *Photinus pyralis* structures [PDB: 1LCI (4) and 1BA3 (5)], which both reportedly crystallized in the primitive tetragonal space group (6) $P4_12_12$. Based on the unit cell volume and molecular weight of 60,844.1 Da, the Matthew's coefficient (V_m) was calculated to be 2.83 $Å^3$/Da which equates to 56.5% solvent content for one molecule in the asymmetric unit. The initial structure of apo luciferase was solved by molecular replacement with MOLREP (6) in the space group $P4_1$ using 1LCI as the search model. Clear peaks were observed from the rotation and translation functions that were approximately 6 and 10 times greater than the background. This along with the observed correlation coefficient of 0.583 indicated that a clear solution had been found. Molecular replacement search in the enantiomorphous space group ($P4_3$) resulted in a correlation coefficient of 0.434 and resulted in high R factors (~50%) following refinement. Therefore, the solution obtained in the space group $P4_1$ was used for refinement. The initial model was refined with Refmac (7) which converged at $R/R_{free} = 21\%$ and 25% and the resulting electron density maps fit well with the overall model. Structures were manually built using Coot (8) and refined with Refmac. The final model was used for molecular replacement against subsequent datasets. Although the adduct complex could be prepared from crystals obtained from both crystallization solutions, those grown from Synergy no. 45, described above, diffracted to moderately higher resolution amongst the samples tested. Therefore, the data collected for the sample from Synergy no. 45 were used for final refinement and model building. For Luc:Apo2 (PDB: 3IER), residual difference electron density was observed in the hydrophobic pocket of the active site and was modeled as a PEG 400 molecule. The following Ramachandran plot statistics were observed: Luc:Adduct (PDB: 3IES): core 91.4%, allowed 8.4%; Luc:Apo (PDB: 3IEP): core 91.5%, allowed 8.2%; Luc:Apo2: core 92.9%, allowed 6.8%.

Liquid chromatography/mass spectrometry (LC-MS). Samples (10 μL injection) were analyzed on an Agilent 1200 series LC-MS equipped a Agilent 6130 Quadrupole MS detector and a Luna C18 reverse phase (3 μ, 3 × 75 mm) column having a flow rate of 1.0 mL/min. The mobile phase was a mixture of acetonitrile (ACN) (0.025% TFA) and H_2O (0.05% TFA), and column temperature was maintained at 50 °C. A gradient of 4% to 100% ACN over 3 min was applied.

MALDI-TOF mass spectrometric analysis. Samples were submitted for analysis by MALDI-MS to determine if the luciferase crystals were composed of the expected 60,844.1 Da protein. Additionally, the protein used for crystallization screening was tested for comparison. Analysis was performed using a MALDI-TOF mass spectrometer (PerSeptive Biosystems, Voyager-DE STR). The instrument was operated in a positive linear mode with following parameters: accelerating voltage 25 kV, grid voltage 95%, guide wire 0.05%, and extraction delay time 50 ns. Acquisition mass range was 5,000–90,000. Raw spectrum data were processed using Gaussian Smooth algorithm within the Data Explorer software (version 4.6). Crystals were transferred from their native drops and washed in three drops of crystallization solution to remove any soluble protein that might be transferred from the crystallization drop before dissolving in 0.1% TFA in water. Protein samples were desalted using reverse phase C4 ZipTips (Millipore) and eluted with 50% acetonitrile/0.1% TFA containing the matrix (sinapinic acid, saturated solution) onto a stainless steel MALDI sample plate. Analysis was performed using a MALDI-TOF mass spectrometer (PerSeptive Biosystems, Voyager-DE STR). The instrument was operated in a positive linear mode with following parameters: accelerating voltage 25 kV, grid voltage 95%, guide wire 0.05%, and extraction delay time 50 ns. Acquisition mass range was 5,000–90,000. Raw spectrum data were processed using Gaussian Smooth algorithm within the Data Explorer software (version 4.6).

Molecular modeling. Fast Rigid Exhaustive Docking (FRED) requires a set of input conformers for each ligand. The multiple low-energy conformers of the ligands were generated by OMEGA and stored in a single binary file. Partial charges were assigned to the ligands using MMFF94 force field (9). The default parameter values were used in OMEGA with two exceptions: the maximal number of low-energy conformations generated for each ligand was set to 1,000, and the rms threshold between different conformers was set to 0.5 Å. The crystallographic structure of luciferase with PTC124-AMP bound was prepared for the docking studies using MOE molecular modeling software [MOE (2008) MOE Molecular Operating Environment (Chemical Computing Group, Montreal]. All hydrogens were added to the protein and partial charges were attributed to the protein atoms using Amber99 force field (10). The docking boxes delineating the binding site were defined by the ligand PTC124-AMP from the luciferase crystal structures using FRED_receptor, a FRED docking preparation program. Each ligand conformation is rigidly optimized using shape and chemical complementarities of protein and ligand, followed by consensus scoring using a number of scoring functions. FRED rigidly docks the pregenerated conformations of each ligand into a nonflexible tar-

get protein to generate an optimal binding pose within the active site through the following consecutive steps: exhaustive docking, systematic solid body optimization of the top ranked candidate poses, ranking pose via consensus structure method, and optionally full coordinate refinement of all ligand atoms using MMFF94 force field. In this work, the force field refinement was not used.

Thermal shift experiments. *P. pyralis* luciferase (FLuc) used in the thermal shift assay was procured from Sigma (catalog no. L1792). The fluorescent dye indicator SYPRO Orange, available at a stock concentration of 5000x, was obtained from Invitrogen, presently Life Technologies. This dye was used due to its low quantum yield in aqueous solution but high fluorescence in nonpolar environments. An increase in fluorescence indicates binding of the dye to hydrophobic regions of the protein which are exposed during protein unfolding. Accurate detection of fluorescent signal in these assays requires the use of high enzyme concentration. The final concentration of the enzyme and SYPRO Orange were maintained at 3.6 μM and 5x, respectively. The enzyme and the dye were separately diluted in either PBS (with or without 2 mM ATP) or Tris-acetate (with or without 2 mM ATP). Test compounds were originally dissolved as 10 mM stock solutions and were further diluted in DMSO, with the exception of the PTC124-AMP adduct which was prepared as 2.9 mM stock in phosphate-buffered saline (PBS, pH 7.4) and was further diluted in either PBS or 50 mM Tris-acetate buffer (pH 7.6). The dilution series were stored in mother plates, serving as source plates for the PCR plates used in the thermal shift experiments. For PTC124 and PTC124 analogs, 1 μL compound solution in DMSO (final concentrations ranging from 0.1 nM to 200 μM) was added to 49 μL FLuc-SYPRO Orange mixture in 96-well thin wall PCR plates (Bio-Rad). The final DMSO content was maintained at the suggested value of 2%. For the PTC124-AMP adduct, 9 μL compound solution (final concentrations: 1–500 μM), or 9 μL buffer as vehicle control, was added to 41 μL FLuc-SYPRO Orange mixture. After sample mixing, the plates were centrifuged at 1,000 rpm for 10 s before being sealed with Optical-Quality Sealing Tape (Bio-Rad). The plates were then heated in an iQ5 Real Time PCR Detection system (Bio-Rad) from 20 to 95 °C in increments of 1 °C and a ramping rate of 0.1 °C/s. The temperature ramp commenced approximately 2 min after sample mixing. Fluorescence intensity changes (Ex 490/Em 575 nm) were monitored with a CCD camera (11).

Analysis of thermal shift data. The temperature midpoint of the protein unfolding transition, T_m, was obtained through a Boltzmann model using an Excel based worksheet provided by Niesen et al. (11):

$$\mathrm{RFU} = \mathrm{RFU1} + (\mathrm{RFU2} - \mathrm{RFU1})/\{1 + \exp[(T_m - T)/\mathrm{slope}]\} \quad \textbf{[S1]}$$

where RFU1 and RFU2 represent the minimum and maximum fluorescence intensities at temperatures at the two sides of the transition, respectively. The differences between the midpoints (T_m) of the thermal profiles of the control (samples with DMSO or carrier buffer without compounds) and compound-containing samples were calculated to yield thermal shifts (ΔT_m).

FLuc enzymatic assays to determine compound potency. Average potency for a given compound is based on at least three experimental replicates performed on different days. IC50 values estimated from compounds that only partially inhibit (i.e., have reduced efficacy against FLuc) are generally of lesser confidence. Compounds were dissolved in DMSO with the exception of adduct (**6**), which was dissolved in PBS.

Cell-based FLuc nonsense codon suppression assays. GripTite™ cells transiently transfected according to standard procedure (TransFast Transfection Reagent; Promega; cat. no. E2431) with the pFLuc190^{UGA} construct were seeded in white solid-bottom tissue culture-treated 1,536-well microplates (Greiner Bio-One) at a density of 6.7×10^5 cells/mL in a volume of 6 μL per well (~4000 cells/well) using the BioRAPTR Flying Reagent Dispenser (FRD; Aurora Discovery). Plates were then incubated for 1 h at 37 °C, 95% humidity, 5% CO_2. These assay plates were then treated with 23 nL of compound or DMSO using a Kalypsys pin tool with a 1,536 array of 10-nL slotted pins. This allowed the delivery of a 24-point titration of each compound to the assay plate, with a final compound concentration ranging from approximately 40 μM to 5 pM. Assay plates were then incubated for 48 h. Following incubation, GripTite cells were washed with Dulbecco s Phosphate Buffered Saline (DPBS) (3x; 7 μL/wash; Invitrogen; 14040) using a Multidrop Combi (Thermo Fisher Scientific) followed by removal of liquid by brief centrifugation. A final volume of 6 μL of DPBS was delivered to each well before addition of 3 μL of 3x detection reagent (contains 100 mM Tris-HCl, 40 mM Tris-Base, 3 mM $MgCl_2$, 3% Triton-X, 15 mM DTT, 1.5 mM CoASH, 450 μM ATP, and 1.4 mM D-luciferin, and prepared in-house) using the FRD. Luciferase activity was then measured using a ViewLux CCD imager (PerkinElmer), with an exposure time of 120 s. Estimates of compound potency were based on an average of at least two experimental replicates performed on different days. An estimate to test the potency of the adduct (**6**) was not conducted, due to stability and solubility issues of the adduct in DMSO, the solvent necessary to deliver compound to cells.

General synthetic methods. Unless otherwise stated, all reactions were carried out under an atmosphere of dry argon or nitrogen in dried glassware. Indicated reaction temperatures refer to those of the reaction bath, whereas room temperature (RT) is noted as 25 °C. All solvents were of anhydrous quality purchased from Aldrich Chemical and used as received. Commercially available starting materials and reagents were purchased from Aldrich, TCI, and Acros and were used as received. If needed, products were purified via a Waters semipreparative HPLC equipped with a Phenomenex Luna C18 reverse phase (5 μ, 30 × 75 mm) column having a flow rate of 45 mL/ min. The mobile phase was a mixture of acetonitrile and H_2O each containing 0.1% trifluoroacetic acid. Samples were analyzed for purity on an Agilent 1200 series LC-MS equipped with a Luna C18 reverse phase (3 μm, 3 × 75 mm) column having a flow rate of 0.8–1.0 mL/ min. The mobile phase was a mixture of acetonitrile (0.025% TFA) and H_2O (0.05% TFA), and temperature was maintained at 50 °C. A gradient of 4% to 100% acetonitrile over 8.5 min was used for purity analysis. Purity of final compounds was determined to be >95%, using a 3 μL injection with quantitation by area under the curve at 220 and 254 nm.

Analytical thin layer chromatography (TLC) was performed with Sigma Aldrich TLC plates (5 × 20 cm, 60 Å, 250 μm). Visualization was accomplished by irradiation under a 254 nm UV lamp. Chromatography on silica gel was performed using forced flow (liquid) of the indicated solvent system on Biotage KP-Sil prepacked cartridges and using the Biotage SP-1 automated chromatography system. ^{1}H– and ^{13}C NMR spectra were recorded on a Varian Inova 400 MHz spectrometer. Chemical shifts are reported in ppm with the solvent resonance as the internal standard ($CDCl_3$ 7.26 ppm, 77.00 ppm, DMSO-d_6 2.5 ppm, 39.51 ppm for ^{1}H, ^{13}C, respectively). Data are reported as follows: chemical shift, number of protons, multiplicity (s = singlet, d = doublet, dd = doublet of doublet, t = triplet, q = quartet, br = broad, m = multiplet), coupling constants. Low-resolution mass spectra (electrospray ionization) were acquired on an Agilent Technologies 6130 quadrupole spectrometer coupled to an Agilent

Technologies 1200 series HPLC. High-resolution mass spectral data were collected in-house using and Agilent 6210 TOF mass spectrometer, also coupled to an Agilent Technologies 1200 series HPLC system.

General synthesis of PTC124 and analogs.

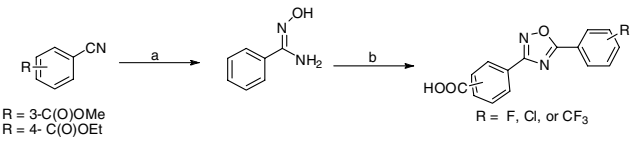

Reagents and conditions: (*a*) NH_2OH, HCl, Hunig's base, CH_2Cl_2, 40 °C, 85–90%; (*b*) (*i*) R-$C_6H_4C(O)Cl$, $(iPr)_2Net$, dimethyl ether (DME), RT; (*ii*) DME, 100 °C; (*iii*) LiOH, 2:1 THF/H_2O, RT, 50–90%.

Synthesis of PTC124 and analogs. The solution-phase synthesis of PTC124 (**1**) was accomplished utilizing methods similar to reported protocols (12, 13). The final three transformations [coupling of (*N′*-hydroxycarbamimidoyl)benzoates with substituted benzoyl chloride, cyclization to form oxadiazole, and ester deprotection] were accomplished using a modified one-pot method.

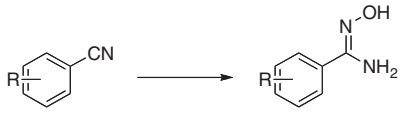

(Z)-alkyl-[3-or-4]-(N′-hydroxycarbamimidoyl)benzoates. To a solution of either methyl 3-cyanobenzoate or ethyl 4-cyanobenzoate (1 equivalent) in ethanol (2 mL/mmol cyanobenzoate) was added hydroxylamine hydrochloride (1.5 equivalents) and diisopropylethylamine (2 equivalents). The mixture was heated to 40 °C and allowed to stir for 18 h, monitored by TLC for the disappearance of starting material. An excess of ice water was then added, and the resulting precipitate was collected via filtration, washed with water and ether, and allowed to dry. No further purification was needed and yields ranged from 85–90%.

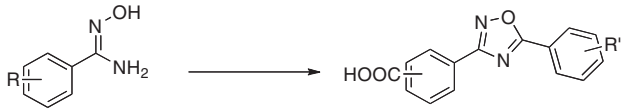

5-Phenyl substituted [3-or-4]-(5-phenyl-1,2,4-oxadiazol-3-yl)benzoic acids. To a solution of either (*Z*)-methyl-3-(*N′*-hydroxycarbamimidoyl)benzoate or (*Z*)-ethyl-4-(*N′*-hydroxycarbamimidoyl)benzoate (1 equivalent) in 1,2-dimethoxyethane (3 mL/mmol) was added diisopropylethylamine (1.5 equivalents) and the solution was cooled to 5 °C. To this mixture was added one of numerous substituted benzoyl chlorides (typical substitutions were F, Cl, and CF_3 at the *ortho*, *meta*, and *para* positions, 1.2 equivalents) dropwise over a 20 min period. The mixture was allowed to warm to RT and was stirred for 4 h. The resulting mixture was heated at 100 °C for 12 h in a sealed reaction vessel. The reaction was then cooled to room temperature, and the solvent was removed under reduced pressure. The crude mixture was taken up in 2:1 THF/water (3 mL/mmol), and lithium hydroxide monohydrate (6 equivalents) was added. The reaction mixture was stirred for 3 h at RT, after which the organic solvent was removed under reduced pressure. The residue was dissolved in ethyl acetate and washed with 10% aqueous HCl. The organic layer was separated, dried ($MgSO_4$), filtered, and concentrated to afford generally pure products after column chromatography. If needed, products were further purified via a Waters semipreparative HPLC equipped with a Phenomenex Luna C18 reverse phase (5 μm, 30 × 75 mm) column having a flow rate of 45 mL/min. The mobile phase was a mixture of acetonitrile and H_2O each containing 0.1% trifluoroacetic acid. Pure fractions were concentrated and dried using Glas-Col N_2 blowdown unit at 40 °C. Typical overall product yields ranged from 40–90%.

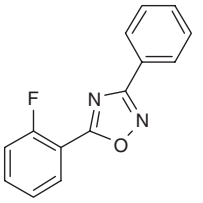

(2). 5-(2-fluorophenyl)-3-phenyl-1,2,4-oxadiazole. See procedure described above.

LC-MS: RT (min) = 6.73; ^{1}H NMR (400 MHz-DMSO-d_6) δ 7.42-7.61 (m, 5H), 7.72-7.78 (m, 1H), 8.05 (m, 2H) and 8.17 (m, 1H); ^{13}C NMR (400 MHz-DMSO-d_6) δ 111.67, 111.79, 117.10, 117.30, 125.33, 125.37, 125.92, 127.06, 129.17, 130.76, 131.60, 135.50, and 135.59; (Additional peaks are due to splitting with *o*-Fluoro group); high-resolution mass spectrometry (HRMS) (*m/z*): $[M]^+$ calculated for $C_{14}H_9FN_2O$, 240.0699; found, 240.0696.

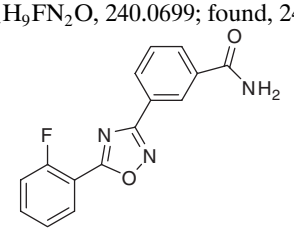

(3). 3-(5-(2-fluorophenyl)-1,2,4-oxadiazol-3-yl)benzamide. To a solution containing 3-(5-(2-fluorophenyl)1-,2,4-oxadiazol-3-yl)benzoic acid (0.150 g, 0.53 mmol) in anhydrous CH_2Cl_2 (4 mL) at 0 °C was added oxalyl chloride (0.092 mL, 1.05 mmol) followed by cat. dimethylformamide (DMF). The reaction mixture was warmed to RT and stirred for 1.5 h. After this time, the reaction mixture was concentrated under reduced pressure and dried under high vacuum. The residue was redissolved in dioxane (4 mL) and 30% NH_3 in water (10 equiv) was added dropwise. After 10 min, the reaction mixture was diluted with ethyl acetate and washed with brine. The organic layer was separated, dried ($MgSO_4$) filtered, and concentrated under diminished pressure. No further purification was required. Yield: 0.148 g, 99%.; LC-MS: RT (min) = 5.12; ^{1}H NMR (400 MHz-DMSO-d_6) δ 7.50 (td, 1H, J = 7.6 and 1.2 Hz), 7.55 (m, 2H), 7.71 (td, 1H, J = 8.0 and 0.4 Hz), 7.81 (m, 1H), 8.11 (m, 1H), 8.24 (m, 3H), and 8.60 (m, 1H); ^{13}C NMR (400 MHz-DMSO-d_6) δ 111.67, 111.78, 117.32, 125.43, 125.58, 126.09, 126.34, 126.43, 129.31, 129.42, 129.68, 130.44, 130.91, 135.30, 135.78, 158.68, 161.24, 166.98, 167.68, 172.62, and 172.66; (additional peaks are due to splitting with *o*-Fluoro group) HRMS (*m/z*): $[M]^+$ calculated for $C_{15}H_{10}FN_3O_2$, 283.0757; found, 283.0759.

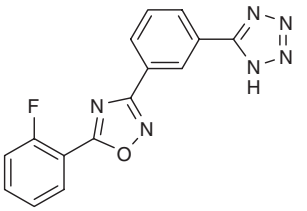

(4). 3-(3-(1H-tetrazol-5-yl)phenyl)-5-(2-fluorophenyl)-1,2,4-oxadiazole. To a solution containing 0.050 g (0.19 mmol) of 3-(5-(2-fluorophenyl)-1,2,4-oxadiazol-3-yl) benzonitrile in DMF (1.5 mL)

was added 0.074 g (1.13 mmol) of sodium azide followed by 0.10 g (1.89 mmol) of ammonium chloride. The reaction mixture was heated to 90 °C for 24 h under a nitrogen atmosphere. After this time, the reaction was cooled to RT, diluted with 0.5 mL of DMSO and filtered through a syringe filter. The filtrate was purified via a Waters semipreparative HPLC equipped with a Phenomenex Luna C18 reverse phase (5 μm, 30 × 75 mm) column having a flow rate of 45 mL/min. The mobile phase was a mixture of acetonitrile and H_2O each containing 0.1% trifluoroacetic acid. The product was collected as a colorless solid after lyophilization: yield 0.052 mg (89%); LC-MS: RT (min) = 5.62; ^{1}H NMR (400 MHz-DMSO-d_6) δ 7.52 (td, 1H, J = 6.8 and 1.2 Hz), 7.57 (ddd, 1H, J = 10.8, 8.4, and 0.8 Hz), 7.81 (m, 1H), 7.85 (t, 1H, J = 7.6 Hz), 8.28 (m, 3H), and 8.78 (t, 1H, J = 1.6 Hz); ^{13}C NMR (400 MHz-DMSO-d_6) δ 111.63, 111.74, 117.23, 117.44, 125.37. 125.51, 125.54, 127.11, 129.52, 129.95, 130.62, 130.92, 135.80, 135.89, 158.69, 161.25, 167.38, 172.77, and 172.81; (additional peaks are due to splitting with *o*-Fluoro group) HRMS (m/z): $[M]^+$ calculated for $C_{15}H_9FN_6O$, 308.0822; found, 308.0823.

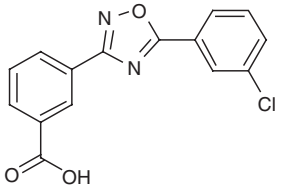

(5). 3-(5-(3-chlorophenyl)-1,2,4-oxadiazol-3-yl)benzoic acid. See procedure described above.

LC-MS: RT (min) = 6.73; ^{1}H NMR (400 MHz-DMSO-d_6) δ 7.68 (t, 1H, J = 8.0 Hz), 7.72 (t, 1H, J = 8.0 Hz), 7.79 (ddd, 1H, J = 8.0, 2.0, and 0.8 Hz), 8.14–8.18 (m, 3H), 8.30 (dt, 1H, J = 8.0 and 1.6 Hz), 8.61 (t, 1H, J = 1.6 Hz), and 13.33 (brs, 1H); ^{13}C NMR (400 MHz-DMSO-d_6) δ 125.08, 126.29, 126.67, 127.40, 127.73, 129.81, 131.07, 131.55, 131.78, 132.27, 133.20, 134.16, 166.45, 167.72, and 174.42; HRMS (m/z): $[M]^+$ calculated for $C_{15}H_9ClN_2O_3$, 300.0302; found, 300.0306.

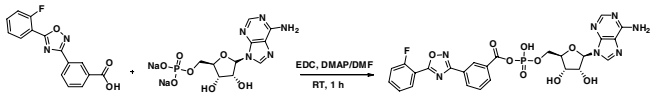

(6). PTC 124-AMP adduct. A mixture of 3-(5-(2-fluorophenyl)-1,2,4-oxadiazol-3-yl)benzoic acid 0.2 g (0.70 mmol) and ethyl-(N′,N′-dimethylamino)propylcarbodiimide (EDC) 0.67 g (3.52 mmol) in anhydrous DMF (4 mL) was stirred at RT for 10 min. Then adenosine-5-monophosphate disodium salt 0.275 g (0.70 mmol) and 4-dimethylaminopyridine (DMAP) 9 mg (0.07 mmol) were added and stirred vigorously at RT for 1 h. The crude product was purified in preparative HPLC and lyophilized to get the free acid as a white powder. The free acid was then dissolved in 0.1 molar ammonium bicarbonate solution and lyophilized to get the ammonium salt of the PTC-AMP adduct. LC-MS: RT (min) = 4.19; ^{1}H NMR (400 MHz-D_2O) δ 4.33–4.52 (m, 4H), 4.66 (t, 1H, J = 5.6 Hz), 5.88 (d, 1H, J = 5.6 Hz), 7.18–7.28 (m, 2H), 7.39 (t, 1H, J = 7.8 Hz), 7.60 (q, 1H, J = 13.6 and 6.8 Hz), 7.71 (s, 1H), 7.80 (t, 1H, J = 7.2 Hz), 7.86–7.91 (m, 2H), 7.95 (s, 1H), 8.13 (s, 1H); ^{13}C-NMR (400 MHz-D_2O) δ 41.5, 66.4, 70.0, 73.9, 83.3, 83.4, 86.5, 110.6, 110.7, 116.8, 117.0, 117.7, 125.0, 125.2, 128.1, 129.2, 129.3, 129.4, 130.2, 131.7, 132.7, 135.7, 135.8, 148.3, 152.1, 154.6, 158.8, 161.3, 162.8, 162.9, 166.7, 172.67, and 172.72; (additional peaks are due to splitting with *o*-Fluoro group); HRMS (m/z): $[M]^+$ calculated for $C_{25}H_{21}FN_7O_9P$, 613.1122; found, 613.1128.

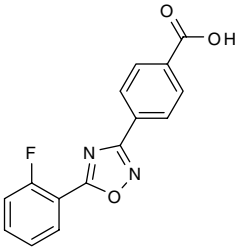

(7). 4-(5-(2-fluorophenyl)-1,2,4-oxadiazol-3-yl)benzoic acid. See procedure described above.

LC-MS: RT (min) = 5.78; ^{1}H NMR (400 MHz-DMSO-d_6) δ 7.49 (td, 1H, J = 7.6 and 0.8 Hz), 7.54 (ddd, 1H, J = 10.8, 8.4, and 0.8 Hz), 7.80 (m, 1H), 8.12 (m, 2H), 8.22 (m, 3H) and 13.27 (brs, 1H); ^{13}C NMR (400 MHz-DMSO-d_6) δ 111.65, 111.76, 117.21, 117.42, 125.49, 125.52, 127.03, 128.28, 128.39, 130.89, 135.73, 135.82, 137.06, 158.68, 161.25, 167.04, 167.51, 172.64, and 172.69; (additional peaks are due to splitting with *o*-Fluoro group) HRMS (m/z): $[M]^+$ calculated for $C_{15}H_9FN_2O_3$, 284.0597; found, 284.0601.

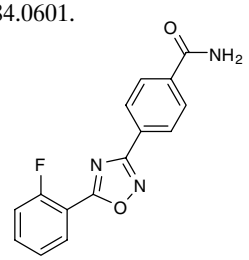

(8). 4-(5-(2-fluorophenyl)-1,2,4-oxadiazol-3-yl)benzamide. See procedure described above.

LC-MS: RT (min) = 5.16; ^{1}H NMR (400 MHz-DMSO-d_6) δ δ 7.49 (td, 1H, J = 7.6 and 0.8 Hz), 7.53 (brs, 1H), 7.55 (ddd, 1H, J = 11.2, 8.4, and 0.8 Hz), 7.80 (m, 1H), 8.06 (m, 2H), 8.15 (m, 3H), and 8.23 (td, 1H, J = 7.6 and 1.6 Hz); ^{13}C NMR (400 MHz-DMSO-d_6) δ 111.65, 111.76, 117.21, 117.42, 125.49, 125.52, 127.03, 128.28, 128.39, 130.89, 135.73, 135.82, 137.06, 158.68, 161.25, 167.04, 167.51, 172.64, and 172.69; (additional peaks are due to splitting with *o*-Fluoro group) HRMS (m/z): $[M]^+$ calcd. for $C_{15}H_{10}FN_3O_2$, 283.0757; found, 283.0755.

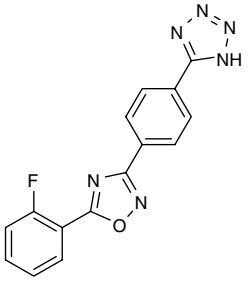

(9). 3-(4-(1H-tetrazol-5-yl)phenyl)-5-(2-fluorophenyl)-1,2,4-oxadiazole. See procedure described above.

LC-MS: RT (min) = 5.63; ^{1}H NMR (DMSO-d_6) δ 7.50 (m, 1H), 7.54 (ddd, 1H, J = 11.2, 8.4, and 1.2 Hz), 7.80 (m, 1H) and 8.20–8.30 (m, 5H); ^{13}C NMR (DMSO-d_6) δ 111.62, 111.73, 117.15, 117.36, 125.46, 125.58, 127.36, 127.77, 128.10, 130.87, 135.72, 155.42, 158.69, 161.26, 167.37, 172.70, and 172.74; (additional peaks are due to splitting with *o*-Fluoro group) HRMS (m/z): $[M]^+$ calculated for $C_{15}H_9FN_6O$, 308.0822; found, 308.0821.

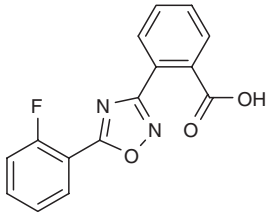

(10). 2-(5-(2-fluorophenyl)-1,2,4-oxadiazol-3-yl)benzoic acid. See procedure described above.

LC-MS: RT (min) = 5.11; ^{1}H NMR (400 MHz-DMSO-d_6) δ 7.48 (td, 1H, J = 8.0 and 1.2 Hz), 7.53 (ddd, 1H, J = 10.8, 8.4, and 0.8 Hz), 7.69–7.81 (m, 4H), 7.81–7.91 (m, 1H), and 8.17 (td, 1H, J = 7.6 and 2.0 Hz); ^{13}C NMR (400 MHz-DMSO-d_6) δ 111.58, 111.70, 117.24, 117.44, 125.52, 125.56, 125.87, 129.53, 130.23, 130.78, 131.11, 131.49, 133.00, 135.67, 135.76, 158.61, 161.18, 167.91, 168.68, 171.55, and 171.59; (additional peaks are due to splitting with o-Fluoro group) HRMS (m/z): $[M]^+$ calculated for $C_{15}H_9FN_2O_3$, 284.0597; found, 308.0593.

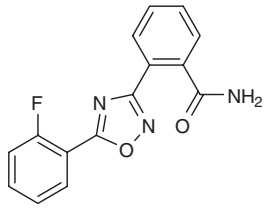

(11). 2-(5-(2-fluorophenyl)-1,2,4-oxadiazol-3-yl)benzamide. See procedure described above.

LC-MS: RT (min) = 4.67; ^{1}H NMR (400 MHz-DMSO-d_6) δ 7.47 (brs, 1H), 7.49 (td, 1H, J, 8.0 and 1.2 Hz), 7.54 (ddd, 1H, J = 10.8, 8.4, and 0.8 Hz), 7.63 (m, 3H), 7.80 (m, 2H), 7.94 (brs, 1H), and 8.17 (td, 1H, J = 7.6 and 1.6 Hz); ^{13}C NMR (400 MHz-DMSO-d_6) δ 111.67, 111.79, 117.22, 117.43, 124.32, 125.49, 125.53, 128.05, 129.72, 129.78, 130.74, 130.80, 135.58, 135.67, 137.87, 158.58, 161.14, 168.43, 169.47, 171.49, and 171.54; (additional peaks are due to splitting with o-Fluoro group) HRMS (m/z): $[M]^+$ calculated for $C_{15}H_{10}FN_3O_2$, 283.0757; found, 283.0756.

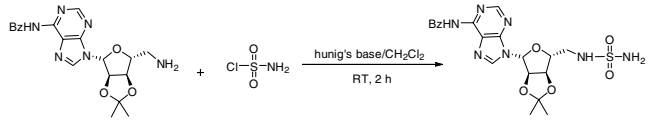

N-(9-((3aR,4S,6R,6aR)-2,2-dimethyl-6-((sulfamoylamino)methyl)tetrahydrofuro[3,4-d][1,3]dioxol-4-yl)-9H-purin-6-yl)benzamide. To a solution containing N-(9-((3aR,4R,6R,6aR)-6-(aminomethyl)-2,2-dimethyltetrahydrofuro[3,4-d][1,3]dioxol-4-yl)-9H-purin-6-yl) benzamide (14–16) (1 g, 1 eq, 2.44 mmol) and Hunig's base (0.85 mL, 2 eq, 4.88 mmol) in dichoromethane (15 mL) was added sulfamoyl chloride (15) (0.422 g, 1.5 eq, 0.85 mL) at 0 °C. The reaction mixture was allowed to stir at RT for 3 h. The solvent was evaporated and the crude product was purified on a Biotage silica gel column using 5% methanol in dichloromethane, providing the product as a colorless solid: yield 0.6 g (2.44 mmol, 47 %). The product was used immediately in the next reaction.

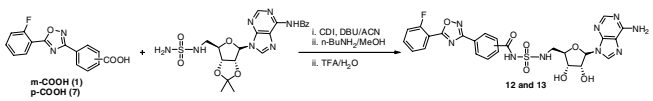

Synthesis of 12 and 13. A 3/4-(5-(2-fluorophenyl)-1,2,4-oxadiazol-3-yl)benzoic acid (**1** or **7**, respectively) (0.969 g, 3.41 mmol, 3 eq) and N,N'-carbonyldiimidazole (0.663 g, 4.09 mmol, 3.6 eq) in acetonitrile (15 mL) was dissolved by heating for 1 h at 60 °C. After cooling, a solution of (0.556 g, 1.136 mmol, 1 eq) and 1,8-diazabicyclo[5.4.0]undec-7-ene (0.26 mL, 1.7 mmol, 1.5 eq) in acetonitrile (15 mL) was added. The reaction mixture was stirred at 60 °C for 1 h. The solvent was evaporated and the crude product was purified on a preparative HPLC. The dry white product was then stirred at RT for 1 h in a mixture of n-butylamine (5 mL) and methanol (5 mL). The solvent was evaporated and the crude product was stirred in a mixture TFA (7 mL) and water (4 mL) at RT for 1 h. The solvent was evaporated and the crude product was finally purified on a preparative HPLC and lyophilized providing the product as a colorless solid.

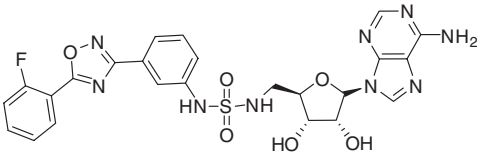

(12). N-(N-(((2R,3S,4R,5S)-5-(6-amino-9H-purin-9-yl)-3,4-dihydroxytetrahydrofuran-2-yl)methyl)sulfamoyl)-3-(5-(2-fluorophenyl)-1,2,4-oxadiazol-3-yl)benzamide. LC-MS: RT (min) = 4.37; ^{1}H NMR (DMSO-d_6) δ 4.12–4.16 (m, 2H), 4.17 (m, 6H), 4.66 (m, 1H), 5.86 (d, 1H, J = 6.4 Hz), 7.48–7.59 (m, 2H), 7.72 (t, 1H, J = 7.6 Hz), 7.78–7.84 (m, 1H), 8.11–8.13 (m, 1H), 8.24–8.32 (m, 2H), 8.37 (s, 1H), 8.48 (s, 1H), 8.57 (t, 1H, J = 1.6 Hz), 8.92 (brs, 1H), and 12.20 (brs, 1H); ^{13}C-NMR (DMSO-d_6) δ 45.1, 71.2, 72.8, 83.7, 88.4, 111.6, 111.7, 119.4, 125.5, 125.6, 126.3, 126.9, 129.7, 130.0, 131.1, 131.2, 132.0, 135.8, 135.9, 148.2, 149.0, 153.4, 158.2, 158.5, 158.7, 161.3, 164.8, 167.4, 172.75, and 172.79; (additional peaks are due to splitting with o-Fluoro group); HRMS (ESI) m/z 612.1419 $(M+H)^+$ ($C_{25}H_{23}FN_9O_7S$ requires 612.1420).

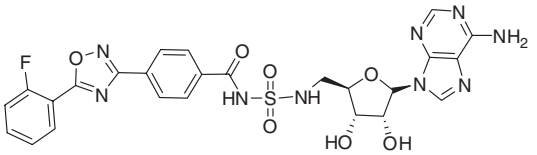

(13). N-(N-(((2R,3S,4R,5S)-5-(6-amino-9H-purin-9-yl)-3,4-dihydroxytetrahydrofuran-2-yl)methyl)sulfamoyl)-4-(5-(2-fluorophenyl)-1,2,4-oxadiazol-3-yl)benzamide. LC-MS: RT (min) = 4.11; ^{1}H NMR (DMSO-d_6) δ 3.62–4.26 (m, 2H), 4.66–4.69 (m, 5H), 7.49–7.59 (m, 2H), 7.79–7.84 (m, 1H, J = 7.6 Hz), 8.09 (d, 2H, J = 8.4 Hz), 8.18 (d, 2H, J = 8.0 Hz), 8.23–8.28 (m, 1H), 8.35 (s, 1H), 8.45 (s, 1H), 8.99 (brs, 1H), and 12.09 (brs, 1H); ^{13}C-NMR (DMSO-d_6) δ 45.16, 71.24, 72.10, 83.64, 88.45, 111.63, 111.74, 114.67, 117.24, 117.45, 119.40, 125.53, 125.60, 127.15, 129.16, 129.58, 130.93, 134.6, 135.83, 135.92, 141.54, 148.29, 149.67, 153.93, 158.71, 161.28, 164.86, 167.30, 172.79, and 172.84; (additional peaks are due to splitting with o-Fluoro group); HRMS (ESI) m/z 612.1423 $(M+H)^+$ ($C_{25}H_{23}FN_9O_7S$ requires 612.1420).

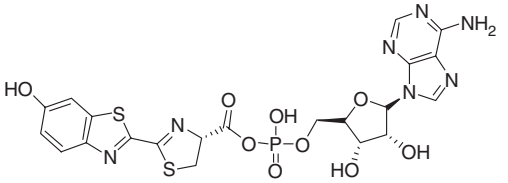

(((2S,3S,4R,5S)-5-(6-amino-9H-purin-9-yl)-3,4-dihydroxytetrahydrofuran-2-yl)methyl phosphoric) (R)-2-(6-hydroxybenzo[d]thiazol-2-yl)-4,5-dihydrothiazole-4-carboxylic anhydride (LH_2-AMP). This compound was prepared, purified, and characterized as reported previously with a few modifications (17, 18). Adenosine-5′-monophosphate (49.5 mg, 0.143 mmol) and D-luciferin (20 mg, 0.071 mmol) were dissolved in DMSO (1 mL), then EDC (274 mg, 1.43 mmol) and DMAP (4.4 mg, 0.036 mmol) in 1 mL DMSO were added and the reaction mixture was stirred for 15 min at RT under argon atmosphere. (All reagents and solvents were bubbled with argon before use.) The crude product was purified using reversed phase preparative HPLC (conditions described in *General synthetic methods*) and lyophilized to get the pure 6.6 mg of LH2-AMP. LC-MS: RT (min) = 2.46 (4.5 min run).

Acknowledgments. Use of the Industrial Macromolecular Crystallography Association Collaborative Access Team beamline 17-BM at the Advanced Photon Source (APS) was supported by the Industrial Macromolecular Crystallography Association through a contract with the Center for Advanced Radiation Sources at the University of Chicago. Use of the APS was supported by the US Department of Energy, under Contract W-31-109-Eng-38.

1. Conti E, Lloyd LF, Akins J, Franks NP, Brick P (1996) Crystallization and preliminary diffraction studies of firefly luciferase from Photinus pyralis. *Acta Crystallogr*, 52(Pt 4):876–878.
2. Otwinowski Z, Minor W (1997) *Processing of X-ray Diffraction Data Collected in Oscillation Mode*. Methods in Enzymology, Macromolecular Crystallography, part A, eds Carter CW, Sweet RM (Academic Press, New York), pp 307–326.
3. Carson M (1997) Ribbons. *Methods Enzymol*, 277:493–505.
4. Conti E, Franks NP, Brick P (1996) Crystal structure of firefly luciferase throws light on a superfamily of adenylate-forming enzymes. *Structure*, 4(3):287–298.
5. Franks NP, Jenkins A, Conti E, Lieb WR, Brick P (1998) Structural basis for the inhibition of firefly luciferase by a general anesthetic. *Biophys J*, 75(5):2205–2211.
6. Vagin AA, Teplyakov A (1997) MOLREP: An automated program for molecular replacement. *J Appl Crystallogr*, 30:1022–1025.
7. Murshudov GN, Vagin AA, Dodson EJ (1997) Refinement of macromolecular structures by the maximum-likelihood method. *Acta Crystallogr* 53(Pt 3):240–255.
8. Emsley P, Cowtan K (2004) Coot: Model-building tools for molecular graphics. *Acta Crystallogr*, 60(Pt 1, Pt 12):2126–2132.
9. Halgren, TA (1996) *J Comput Chem*, 17:490–519
10. Case DA, et al. (2005) The Amber biomolecular simulation programs. *J Comput Chem* 26:1668–1688.
11. Niesen FH, Berglund H, Vedadi M (2007) The use of differential scanning fluorimetry to detect ligand interactions that promote protein stability. *Nat Protoc*, 2(9):2212–2221.
12. Almstead NG, Hwang PG, Pines S, Moon Y, Takasugi JJ (2008) Processes for the preparation of 1,2,4-oxadiazole benzoic acids. #WO 2008/030570.
13. Welch EM, et al. (2007) PTC124 targets genetic disorders caused by nonsense mutations. *Nature*, 447(7140):87–91.
14. Brown P, et al. (1999) Molecular recognition of tyrosinyl adenylate analogues by prokaryotic tyrosyl tRNA synthetases. *Bioorg Med Chem Lett* 7(11):2473–2485.
15. Somu RV, et al. (2006) Rationally designed nucleoside antibiotics that inhibit siderophore biosynthesis of Mycobacterium tuberculosis. *J Med Chem*, 49(1):31–34.
16. Wang T, et al. (2007) Design, synthesis, and molecular modeling studies of 5′-deoxy-5′-ureidoadenosine: 5′-ureido group as multiple hydrogen bonding donor in the active site of S-adenosylhomocysteine hydrolase. *Bioorg Med Chem Lett*, 17(16):4456–4459.
17. Goto T, Imai K (1988) Improved synthesis of firefly D-luciferyl-D-adenylate-A key intermediate of firefly bioluminescence. *Agric Biol Chem*, 52(11):2803–2809.
18. Viviani VR, Ohmiya Y (2006) Bovine serum albumin displays luciferase-like activity in presence of luciferyl adenylate: Insights on the origin of protoluciferase activity and bioluminescence colours. *Luminescence*, 21(4):262–267.
19. Fraga H, Fernandes D, Fontes R, Esteves da Silva JC (2005) Coenzyme A affects firefly luciferase luminescence because it acts as a substrate and not as an allosteric effector. *FEBS J*, 272(20):5206–5216.
20. Nakatsu T, et al. (2006) Structural basis for the spectral difference in luciferase bioluminescence. *Nature*, 440(7082):372–376.
21. Rhodes WC, McElroy WD (1958) The synthesis and function of luciferyl-adenylate and oxyluciferyl-adenylate. *J Biol Chem*, 233(6):1528–1537.
22. Shrake A, Ross PD (1988) Biphasic denaturation of human albumin due to ligand redistribution during unfolding. *J Biol Chem*, 263(30):15392–15399.
23. Celej MS, Montich GG, Fidelio GD (2003) Protein stability induced by ligand binding correlates with changes in protein flexibility. *Protein Sci*, 12(7):1496–1506.
24. Shrake A, Finlayson JS, Ross PD (1984) Thermal stability of human albumin measured by differential scanning calorimetry. *Vox Sang*, 47(1):7–18.
25. Shrake A, Ross PD (1990) Ligand-induced biphasic protein denaturation. *J Biol Chem*, 265(9):5055–5059.

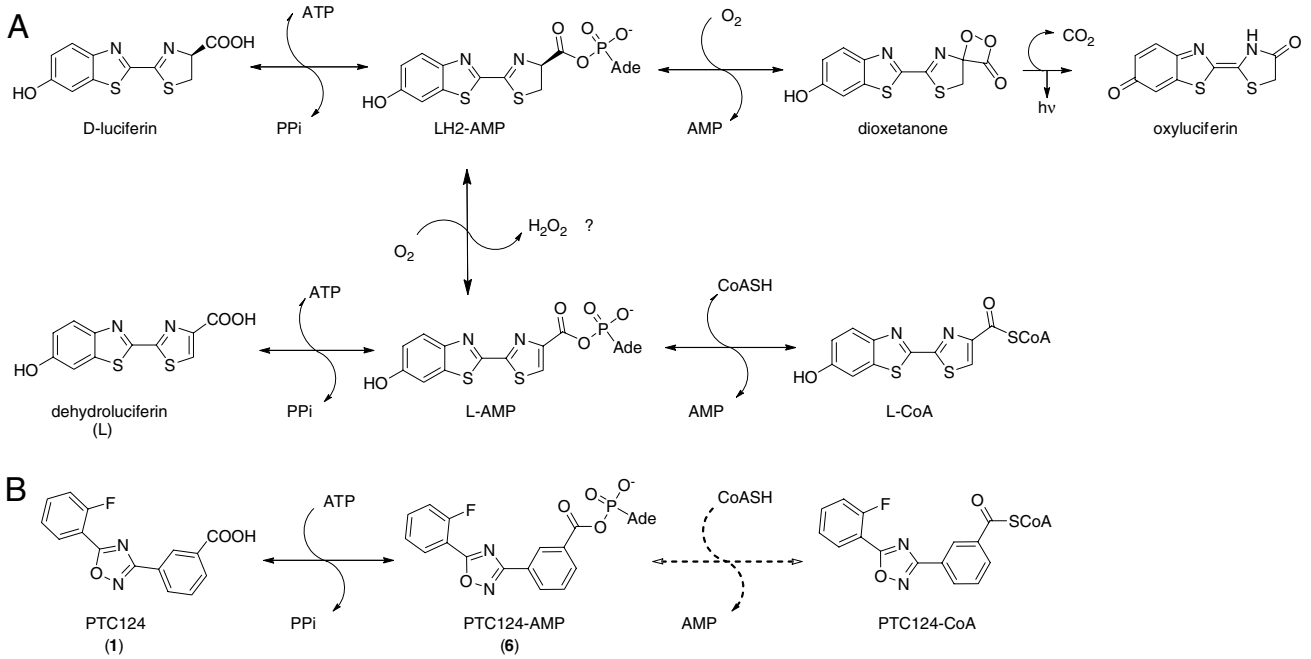

Fig. S1. Reactions catalyzed by FLuc. (*A*) FLuc catalyzes the reaction between D-luciferin and ATP to form the intermediate LH_2-AMP which eventually leads to production of oxyluciferin and light. A side-reaction involving oxidation of the LH_2-AMP intermediate forms L-AMP, which is an inhibitor of FLuc (specifically, an MAI). The "?" indicates that the exact mechanism of oxidation and the efficiency of this conversion is presently unknown. Potent inhibition of FLuc by L-AMP can be relieved through the thiolytic reaction of FLuc-bound L-AMP and coenzyme A (CoASH), to form L-CoA, a significantly weaker inhibitor of FLuc (19). Figure adapted from Fraga et al. (19). (*B*) FLuc enzyme catalyzed reaction of PTC124 and ATP to form the potent MAI PTC124-AMP. We predict that thiolysis can also occur between PTC124-AMP and CoASH, similar to that reported for L-AMP and CoASH, forming a PTC124-CoA product, which is significantly less inhibitory than PTC124-AMP.

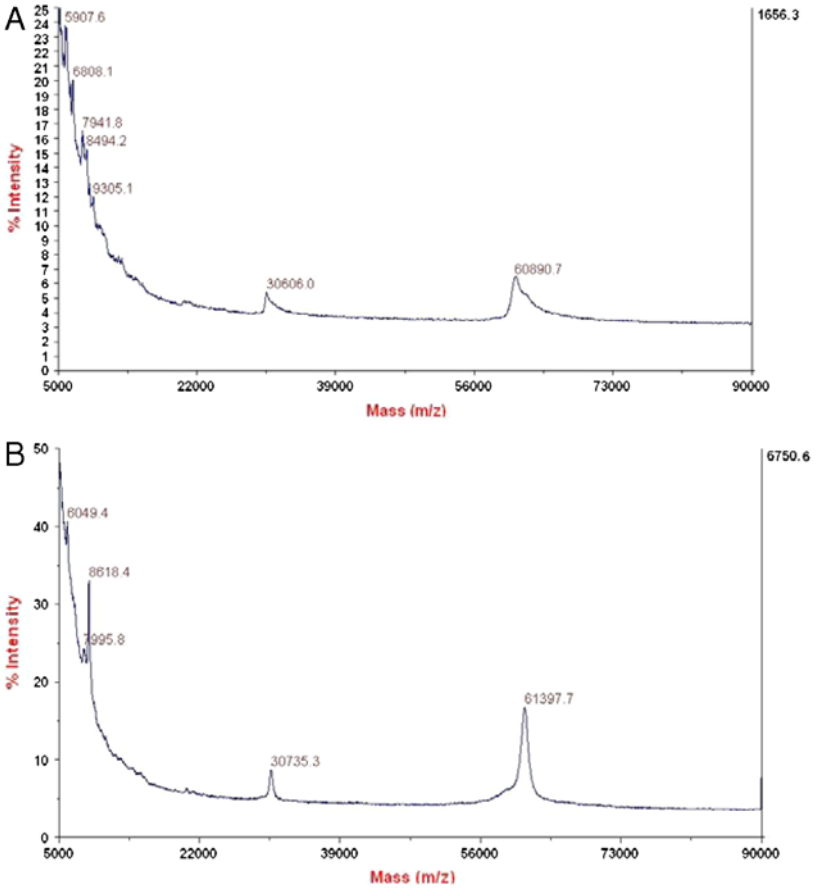

Fig. S2. MALDI-MS of FLuc. (*A*) Luciferase purchased from Sigma. (*B*) Luciferase crystals obtained from Synergy no. 45 dissolved in 0.1% TFA/water. For the luciferase structure described here, we found that the residues in the C-terminal domain region near V435 to V551 in the full length model used for molecular replacement were not masked by electron density following refinement. In addition, the *B* factors for the amino acids in this region refined to approximately 6 times that of the average value of the model indicating that these residues were disordered. The protein used for crystallization experiments, as well as the FLuc crystals themselves, displayed a peak near the expected 60 kDa molecular mass of FLuc, indicating that the C-terminal residues were indeed disordered and not truncated. This is not unexpected as the C-terminal domain appears to be dynamic when comparing previously determined structures of luciferase. For example, the structures from LcrLuc (20) and FLuc (4) are rather similar overall, whereas the C-terminal domains adopt dramatically different orientations relative to each other.

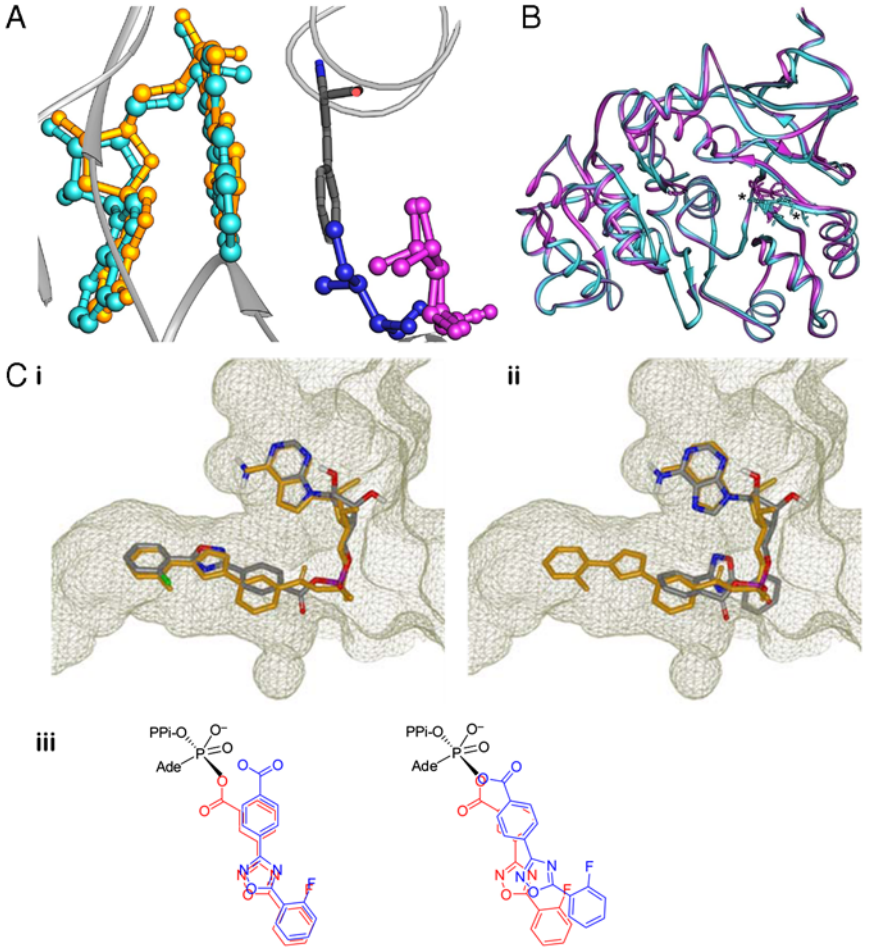

Fig. S3. Comparison of FLuc structures and modeling of the PTC124-AMP adducts. (*A*) Overlay of PTC124-AMP (*Turquoise*) and LcrLuc bound to DLSA (*Gold*; PDB: 2D1S) showing the similarities of the ligand binding mode. Ile 288 from LcrLuc:DLSA is colored blue and Leu 286 from the FLuc structures (apo and bound) are colored magenta. Phe 247 from FLuc is shown in dark gray. Structures shown are rotated approximately 90° relative to Fig. 2*C* shown in the main text. (*B*) Overlay of FLuc:PTC124-AMP (*Turquoise*) with FLuc:Apo (*Magenta*). The overall structures are quite similar with the exception of the loop region between Ser 314 and Leu 319 located between the asterisks. We also determined a second apo structure of FLuc (FLuc:Apo2; see PDB: 3IER), one that contains a polyethylene glycol 400 (PEG 400) molecule (a component of the crystallization solution) bound in the hydrophobic luciferin pocket. The binding of PEG 400 does not affect the conformation of the loop between Ser 314 and Leu 319, which is nearly identical to FLuc:Apo. For example, Ala 317 was disordered in FLuc:Apo2, and thus could not be modeled, and the *B* factors for residues in this loop are nearly twice that of the average value of the model for apo structures unlike the PTC-AMP bound structure, where the *B* factors for this loop are similar to the overall value for the model, with well-defined electron density. (*C*) The *para*- and *ortho*-PTC124-AMP adducts (*i*, *ii*, respectively) were modeled in the binding pocket defined by the cocrystal structure of the PTC124-AMP adduct (gold structure). Molecular docking of the *para*- and *ortho*-PTC124-AMP adducts were performed using FRED. See *SI Methods* for details. This figure was prepared with the program VIDA (OpenEye Scientific Software). (*C, iii*) illustrates how in the active site the carboxylate oxygen of PTC124 (*m*-isomer, shown in red) is ideally situated to form a near-attack conformer (NAC) and displace pyrophosphate from ATP. However, when the diphenyloxadiazole moiety of the *p*-isomer (*Blue*) is superimposed over that of the *m*-isomer (*Left*), the nucleophilic oxygen is too far away to form an efficient NAC. To locate the nucleophilic oxygen of the *p*-isomer requires a realignment of the long axis of the molecule by *ca.* 20° as shown on the right. Hence, the *p*-isomer is much less effective than the *m*-isomer in undergoing MAI formation.

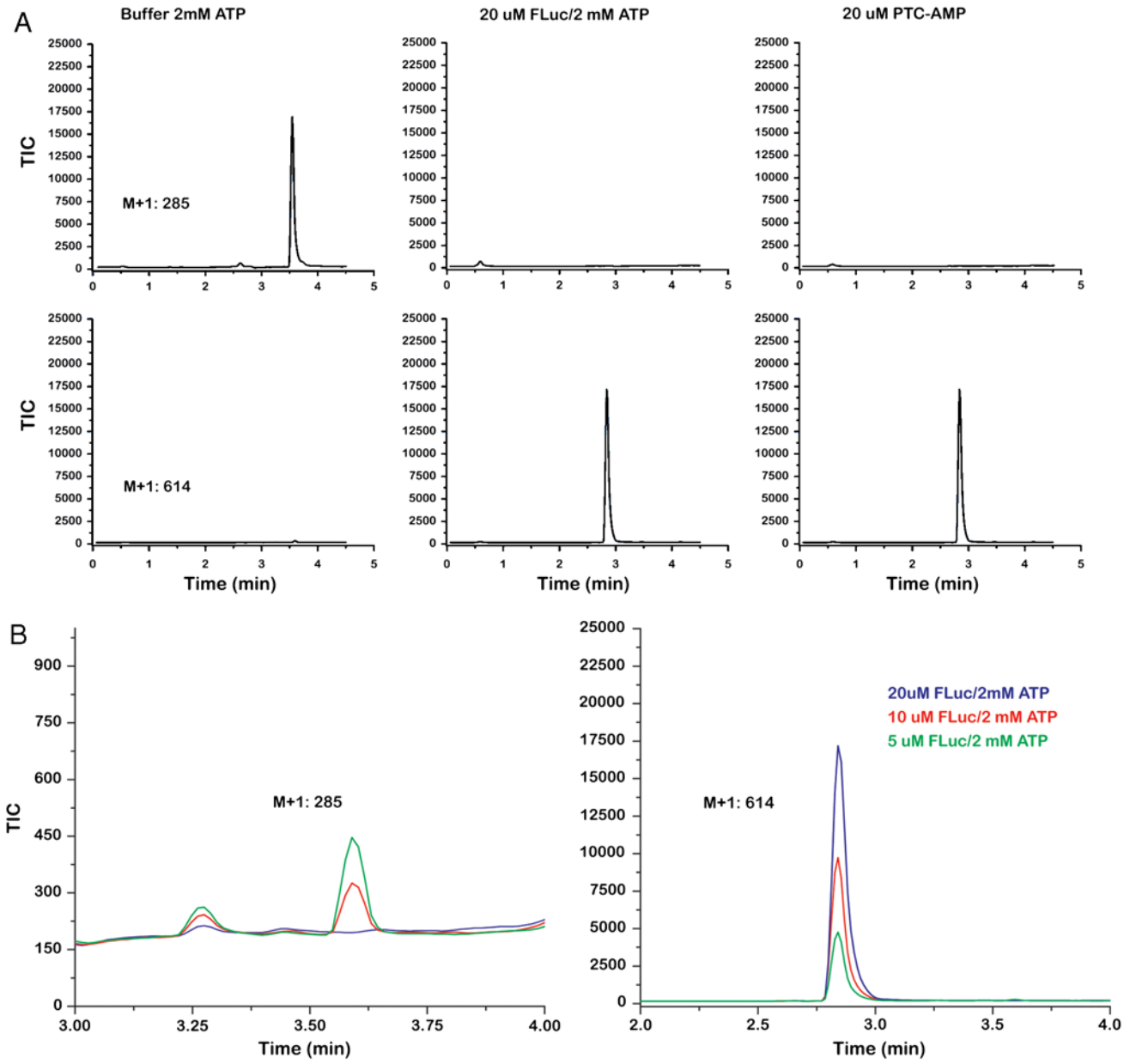

Fig. S4. LC-MS analysis of adenylate adduct formation by FLuc. (*A*) Far left and middle graphs show the total ion current (TIC) data (PTC124 mass, *Top Graphs*; PTC124-AMP mass, *Bottom Graphs*) for incubation of 20 μM PTC124 in the presence of 2 mM ATP alone or with 20 μM FLuc and 2 mM ATP. The far right graph shows the TIC data for the synthetically made PTC-AMP in buffer alone. (*B*) The formation of PTC-AMP can be titrated by varying the enzyme concentration. The TIC for the PTC124 (*Left Graph*) and PTC-AMP (*Right Graph*) is shown at three different FLuc concentrations with 2 mM ATP present and 20 μM PTC124, incubation time ~10 min.

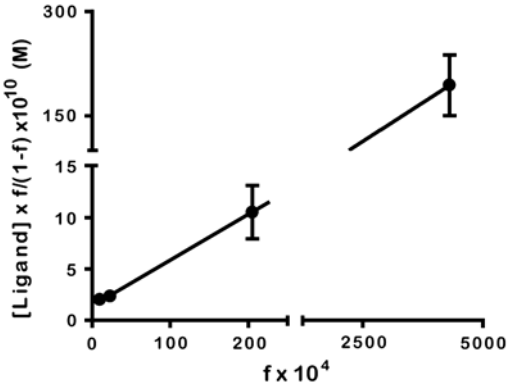

Fig. S5. K_D determination for the PTC124-AMP:FLuc complex. A method to calculate the K_D defined as $K_D = \frac{(E)_{free}(\text{PTC124-AMP})_{free}}{E\text{-PTC124-AMP}}$ used the derivation described by Rhodes and McElroy (21) where we applied the following linear equation to obtain the K_D: $K_D = \frac{f}{1-f}(\text{PTC124-AMP})_{total} - f(E)_{total}$, where $f = \frac{E_{free}}{E_{total}}$. The fraction ($f$) is directly calculated from the ratio of light intensities upon incubation of FLuc with LH_2-AMP at varying concentrations of PTC124-AMP ligand. In the experiment, known concentrations of PTC124-AMP are added to a known concentration of FLuc (100 nM) and the light intensity is measured immediately after addition of LH_2-AMP. From this linear plot E_{total} and K_D are obtained from the slope and intercept of the graph, respectively. From the plot shown, we obtained an $E_{total} = 43$ nM and a $K_D = 143$ pM (average 130 ± 20 pM); r^2 for plot is 1.000. Ligand = PTC124-AMP.

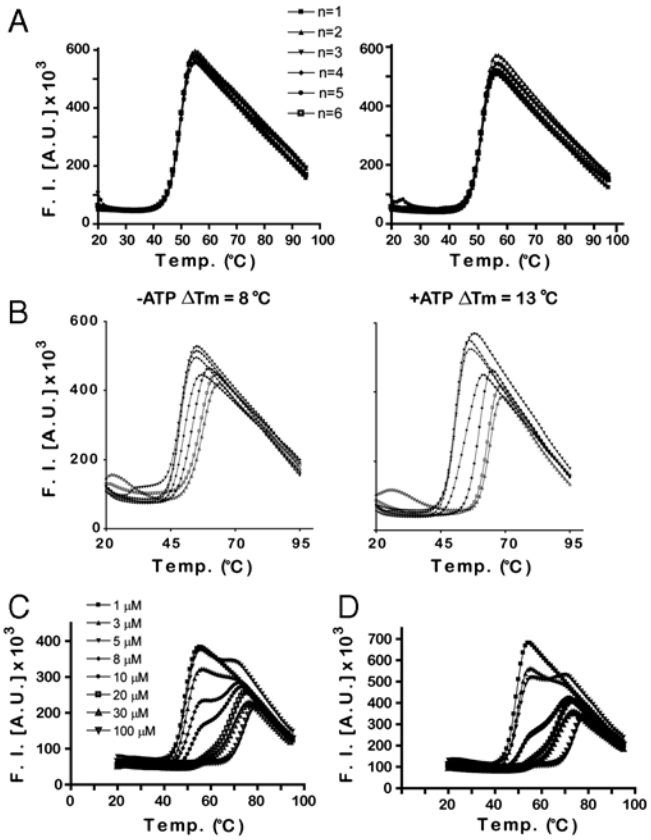

Fig. S6. Thermal shift profiles. We assessed the thermal profile of 3.6 μM FLuc in Tris-acetate buffer and obtained a T_m of 48.3 °C ± 0.13 (a T_m of 48.5 °C ± 0.11 was obtained for FLuc in PBS). Data shown are for a total of six replicates in all cases and the concentrations of the tested compound are noted in *C*. (*A*) Thermal shift profile of 3.6 μM FLuc in the absence (*Left*) and the presence (*Right*) of 2 mM ATP. Shown are the individual profiles obtained from six replicates (*n*). (*B*) PTC124 thermal melting profiles in the absence (*Left Graph*) and presence (*Right Graph*) of 2 mM ATP at various concentrations of PTC124 ranging from 0.01 to 200 μM (alternate traces shown; see PubChem Assay Identifier: 2309). A concentration-dependent increase in FLuc T_m was observed: marginal (<1.5 °C) T_m shift was detected below 1 μM compound, but the thermostability of the protein was augmented as the compound:protein ratio was increased, reaching a maximal stability (max ΔT_m) near the highest compound concentration tested (200 μM). Thermal denaturation of 3.6 μM FLuc in the presence of increasing concentrations PTC-AMP in Tris buffer (*C*) or PBS buffer (*D*). For this compound, in the 5–20 μM range, biphasic thermal melt curves were observed. At the next higher concentration, 20 μM, the two transitions coalesced yielding a single asymmetric peak which was skewed to the high-temperature side. Such behavior has been previously reported for *Cypridina* luciferase using different detection methods as well as with other proteins, such as undefatted albumin with palmitate (22) and BSA with bis-ANS (23), and has been attributed to an increase in free ligand concentration due to the release of previously bound ligand by the protein during heat denaturation. The resulting redistribution of ligand occupies a lower-affinity site which is revealed at the higher temperatures (24, 25).

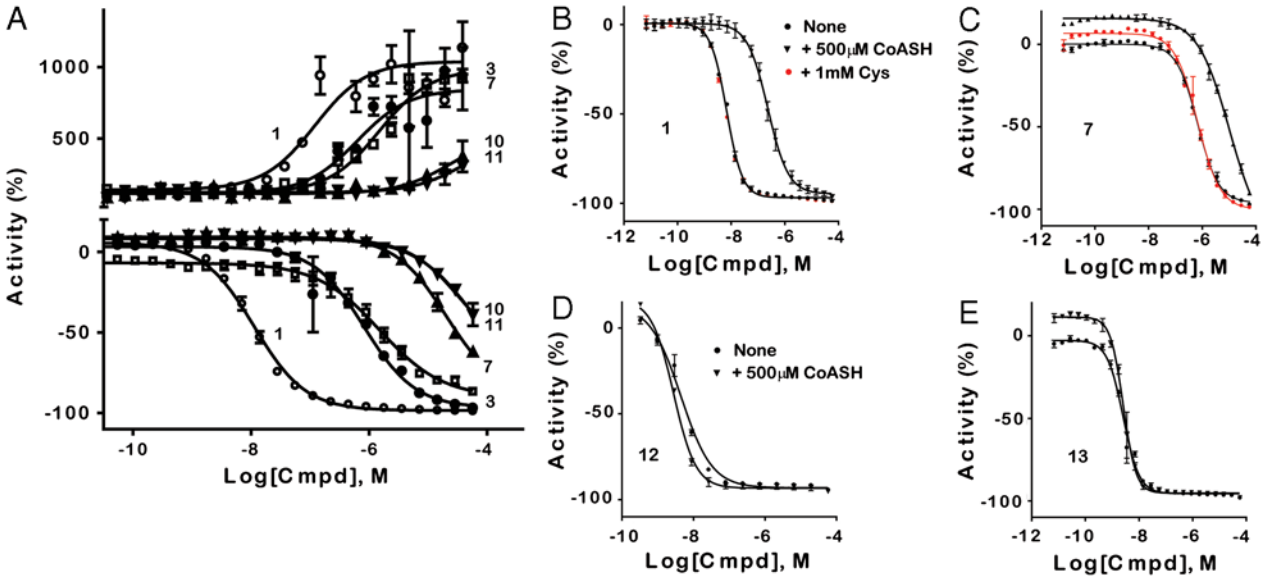

Fig. S7. Example of concentration-response curves for PTC124 and selected analogs in the cell-based nonsense codon suppression assay and in the purified FLuc biochemical assay. (*A*) (*Top*) Cell-based pFLuc190^{UGA} nonsense codon suppression assay. Apparent activation of FLuc activity in the cell-based assay after 48-h incubation of cells with PTC124 or analogs. The most potent compound is PTC124 (**1**) and the least potent compounds, which also demonstrate the weakest efficacies, are the *ortho*-substituted analogs (**10**, **11**). This potency trend is mirrored in the purified enzyme assay (*Bottom*). (*B–E*) Purified enzyme assay, concentration-response curves in the presence or absence of 500 μM CoASH or 1 mM cysteine for PTC124 (**1**; *B*), and the *p*-carboxylate analog (**7**; *C*). CoASH appears to have the greatest effect on the potency of PTC124 (**1**; *B*), and little effect on the acylsulfamide *meta*- and *para*-adducts (**12** and **13**; *D* and *E*) consistent with a thiolytic mechanism.

Table S1. Data collection and refinement statistics

	Luc:PTC124-AMP (PDB: 3IES)	Luc:Apo (PDB: 3IEP)	Luc:Apo2 (PDB: 3IER)
Data collection			
Space group	$P4_1$	$P4_1$	$P4_1$
Cell dimensions			
a, *b*, *c*, Å	83.65, 83.65, 97.10	84.69, 84.69, 96.84	84.23, 84.23, 96.91
α, β, γ, °	90, 90, 90	90, 90, 90	90, 90, 90
Resolution, Å	50 – 2.0 (2.07 – 2.0)*	50 – 2.1 (2.18 – 2.1)*	50 – 2.05 (2.12 – 2.05)*
R_{sym} or R_{merge}	0.107 (0.494)	0.132 (0.518)	0.123 (0.479)
$I/\sigma I$	12.6 (2.3)	11.3 (2.7)	11.1 (2.2)
Completeness, %	98.8 (97.3)	99.9 (100.0)	99.6 (98.7)
Redundancy	5.0 (4.6)	5.1 (5.0)	4.9 (4.2)
Refinement			
Resolution, Å	50 – 2.0	50 – 2.1	50 – 2.05
No. reflections	42,282	37,872	39,997
R_{work}/R_{free}	0.182/0.218	0.188/0.221	0.183/0.225
No. atoms			
Protein	3,384	3,353	3,360
Ligand/ion	43		10
Water	234	199	197
B factors, Å^2			
Protein	22.9	30.8	23.6
Ligand/ion	22.0		39.6
Water	31.4	36.9	29.6
rms deviations			
Bond lengths, Å	0.013	0.018	0.023
Bond angles, °	1.430	1.603	1.926

*Values in parentheses are for highest-resolution shell.

Table S2. Effect of potency with CoASH or Cys on selected compounds

R1	R2		FLuc, μM	FLuc + CoASH, μM	FLuc + Cys, μM
o-F	*m*-COOH	(**1**)	0.014 ± 0.008	0.32 ± 0.21	0.0082 ± 0.003
o-F	*p*-COOH	(**7**)	0.72 ± 0.45	6.2 ± 1.1	0.36 ± 0.25
o-F	*m*-CONH (sa-Ade)	(**12**)	0.005 ± 0.001	0.003 ± 0.001	ND
o-F	*p*-CONH (sa-Ade)	(**13**)	0.003 ± 0.001	0.003 ± 0.001	ND

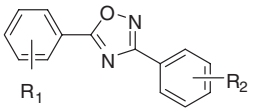

Shown are the averages ±SD from at least two experimental replicates performed on different days. Because CoASH did not appear to have a significant effect on the potency of the two adducts tested (**12**, **13**), the effect of 1mM cysteine was not determined. ND, not determined; sa-Ade, acylsulfamide adenosine.